Shear Forces between Tethered Polymer Chains as a Function of Compression, Sliding Velocity, and Solvent Quality

Phillip A. Schorr,[†] Thomas C. B. Kwan,[‡] S. Michael Kilbey II,[§] Eric S. G. Shaqfeh,*[,‡,||] and Matthew Tirrell[⊥]

Department of Chemical Engineering and Materials Science, University of Minnesota, Minneapolis, Minnesota 55455; Department of Chemical Engineering, Stanford University, Stanford, California 94305; Department of Chemical Engineering, Clemson University, Clemson, South Carolina 29634; Department of Mechanical Engineering, Stanford University, Stanford, California 94305; and Department of Chemical Engineering, University of California—Santa Barbara, Santa Barbara, California 93106

Received July 11, 2001; Revised Manuscript Received September 11, 2002

ABSTRACT: The shear forces between polystyrene chains end-tethered to opposing surfaces have been measured with the surface forces apparatus (SFA) in both good and near-Θ solvents. When the shearing velocity was varied, the complex polymer/solvent system responded in a Newtonian-like fashion with the shear force increasing linearly with the shear velocity. The effective viscosity of the end-tethered systems in this Newtonian-like regime was found to be an order of magnitude greater than the viscosity of semidilute solutions of equivalent molecular weight free chains. At larger shear velocities or higher extents of compression, Brownian dynamics simulations suggest the interfacial width will thin, leading to a sublinear increase in the shear force with sliding velocity. Experimental limitations prevented exploration of the higher shear velocities simulated with the Brownian dynamics approach, but increasing confinement eventually did lead to sublinear behavior, in agreement with the simulation prediction.

Introduction

When simple fluids, such as low molecular weight organic solvents, are compressed to a film thickness on the order of a few molecular monolayers, they undergo a sharp liquid-to-solid transition.[1−3] The mechanism of this transition is an ordered layering of the fluid molecules parallel to the confining surfaces. One consequence of this liquid-to-solid transition is that the simple fluid can now support a normal load.[1,2] Another is that when sheared, the ordered fluid layer exhibits a finite yield stress and a stick−slip response.[2,3] These well-documented effects suggest that simple fluids do not work well as lubricating agents in confined spaces, or when a normal load exists between the sliding surfaces.

One solution to this problem is to end-tether polymer chains to the opposing interfaces. In addition to providing a barrier layer above the surfaces, tethered polymer chains have been recently found to act as effective lubrication modifiers. Experimental work over the past 10 years has suggested that the entropy of the polymer chains provides a fluid layer that can support large normal loads before shear forces are felt between sliding surfaces.[4−13] Tailoring the dynamic properties of these systems, however, is an emerging area of research. While there are indications that frictional interaction between the solvent and segments of the brush controls the strength of the shear response,[6−8] the shear properties of polymer brushes, especially as a function of solvent quality, have yet to be quantitatively predicted by current theoretical models.

Although the normal forces between polymer brushes in a good solvent are fairly well understood, the lateral forces between sliding surfaces have only recently started to be experimentally explored. Klein et al.[9−11,13] found that for opposing polystyrene brushes in toluene, an extremely large normal load could be imposed without detecting any shear forces between the layers. They suggested that the weak interpenetration between the well-solvated brushes allowed the interface to remain fluid and offer little resistance to the shearing motion. When the brushes were compressed further to separation distances less than about 20% of their equilibrium height, the shear forces increased rapidly with compression. This dramatic rise in shear force was attributed to the rapid increase in the viscosity of polystyrene at high concentrations (related to its approach to a glassy state). The idea that shear forces become detectable when the PS layer starts to vitrify has been given some support by the SFA measurements of Pelletier et al.[12] They found that the average chain relaxation time in a good solvent was near 10^{-2} s at the onset of measurable lateral forces and increased rapidly with compression.

When exposed to near-Θ solvents, the lateral forces between polymer brushes have been shown by Granick et al.[14−16] and Kilbey et al.[6−8] to exhibit a very different type of response. The onset of shear forces between PS brushes was found to occur at separation distances comparable to the brush height, rather than requiring a large extent of compression. Because excluded volume repulsions are weakened, Granick et al. suggested that, in contrast to the good solvent case, a high degree of mutual interpenetration developed in the periphery of the brushes. The large shear force required to slide the two brushes past one another was then argued to arise from dissipation induced by chain entanglements in the relatively large interfacial region. Kilbey et al. later suggested that potential differences in the interfacial

* Corresponding author.
[†] University of Minnesota.
[‡] Department of Chemical Engineering, Stanford University.
[§] Clemson University.
[||] Department of Mechanical Engineering, Stanford University.
[⊥] University of California—Santa Barbara.

10.1021/ma011207v CCC: $25.00
Published on Web 12/21/2002

Table 1. PS/PVP Block Copolymer Characterization

block copolymer	M_n PS block GPC data, g/mol	PI of PS block GPC data	M_n copolymer GPC data, g/mol	M_n PVP block GPC data,[a] g/mol	M_n PVP block NMR data,[b] g/mol
PS/PVP[25/4]k	24 900	1.10	28 500	3600	4500
PS/PVP[255/24]k	255 100	1.06	278 900	23 800	23 400

[a] Calculated by subtraction of PS block molecular weight from the diblock molecular weight. [b] Calculated based on relative peak intensities of protons in PS and PVP blocks.

width with solvent quality were not as important as the changes in polymer/solvent interaction strengths. The authors drew parallels with bulk rheology work[17−20] where decreasing the solvent quality was found to lead to an increase in the monomeric friction coefficient for polystyrene solutions at similar concentrations.[17]

Up to this point, only Grest has performed molecular dynamics simulations to explore how degree of compression, velocity and solvent quality impact shear forces between polymer brushes.[4,5,21] (We note that since the submission of the present work, an additional relevant paper by Kreer et al.[22] has appeared.) He found that opposing brushes only weakly interpenetrate and easily slide past one another with immeasurably small shear force at low compression. For higher compressions in his simulation, the shear force rises dramatically in agreement with the experimental work of Klein et al. and Kilbey et al. described earlier. Examining the change in the shear force as a function of the applied velocity at three large compressions, he found that the shear force increases sublinearly with velocity for all three compressions except at very small velocities, where he speculated the existence of a linear Newtonian-like regime. After mapping his dimensionless units, Grest concluded that it was likely that the SFA was capable of probing only the low velocity Newtonian-like regime due to limitations on sliding amplitude and frequency. This could not be verified because there were no experimental data available until now for the velocity dependence of the shear force between polymer brushes using the SFA. In his simulations, Grest also never observed a transition from a linear to a sublinear relationship between the shear force and velocity due to compression because he only operated in the high-compression and high-velocity regime. When Grest modified the interaction potential of the beads in his molecular dynamics simulation to probe the effect of solvent quality,[5] he was able to capture the expected change in the range of the normal forces, with the near-Θ solvent brush being shorter and more compact. Surprisingly, however, the shear forces in the two cases were nearly identical.

To further explore some of these questions, the shear response between polymer brush layers was studied as a function of solvent condition, degree of compression and sliding velocity using the SFA direct force measurement technique. The brush bearing surfaces were made by preferential adsorption of polystyrene−poly(vinyl pyridine) diblock copolymers from a dilute toluene solution onto mica substrates. Parallel lateral motion (low amplitude shear) was imparted to one surface, while the response was detected at the opposing brush-covered surface. Although the SFA can provide an accurate measurement of the forces between two layers, it cannot provide direct information on the internal structure of the tethered chains or the molecular mechanisms involved in the translation of the forces. Therefore, to gain better physical insight into our experimental results, we have also performed Brownian dynamics simulations of two opposing brushes. The parameters of the simulation were chosen to closely mirror those obtained experimentally, so that a qualitative understanding of the SFA data would emerge.

Experimental Section

Materials. The ASTM V-2 Muscovite mica used as the substrate in the surface forces experiments was obtained from S&J Trading of New York and cleaved to sheets 1−3 μm in thickness. Spectroscopic grade toluene and cyclohexane were first redistilled and then filtered through a 0.22 μm Millipore filter prior to use. Two different polystyrene−poly(vinylpyridine) diblock copolymers (PS/PVP) were anionically synthesized following the procedure of Levicky.[23] Briefly, the vinylpyridine and styrene monomers were dried over calcium hydride and then vacuum distilled to separate flasks for further purification. The styrene was then stirred over triethyl aluminum and the vinylpyridine over *n*-butylmagnesium to further remove water and other impurities. After degassing several times, the monomers were distilled into flame-dried, graduated burets for use in the reaction. The anionic polymerization was performed in tetrahydafuran (THF) at a temperature of −70 °C. *sec*-Butyllithium initiator was carefully titrated, and the volume required to obtain the desired PS block molecular weight was added to the THF in the reaction vessel. The styrene monomer was then added dropwise to the reactor. After completion of the styrene polymerization, a small quantity of polymer solution was withdrawn from the reactor. This aliquot was treated with methanol to terminate the living anionic species and stored for later characterization. The proper amount of vinylpyridine was then added to the reaction vessel to give the desired composition of block copolymer. Upon completion of the vinylpyridine polymerization, the reaction was terminated with methanol, and the finished copolymer was recovered by adding the THF solution dropwise into hexane. The molecular weight and composition of the PS/PVP block copolymers were determined using gel permeation chromatography (GPC) and nuclear magnetic resonance (NMR) spectroscopy. The final results of the PS/PVP block copolymer characterization are presented in Table 1.

Self-Assembly Procedure. Bulk polymer solutions of PS/PVP in toluene were prepared with a concentration of 0.06 mg/mL (approximately 60 ppm). This concentration was chosen since it falls near or below the critical micelle concentration (cmc) of PS/PVP in toluene (80 ± 20 ppm depending on the molecular weight and degree of asymmetry of the block copolymer).[24,25] The solutions were allowed to equilibrate for at least 48 h before use in an experiment. The SFA chamber was then filled by passing the block copolymer solution through a 0.22 μm filter. Once filled, the opposing mica surfaces were separated to approximately 1 cm to allow the unhindered adsorption of PS/PVP to commence. At least 18 h were allowed for the polymer to adsorb from toluene onto the mica surfaces in the SFA before force profiles were measured. Previous studies of PS/PVP adsorption onto mica have indicated that saturation of the substrate occurs well within this allotted period of time.[24] Since toluene is a good solvent for PS and a poor solvent for PVP, the PVP block preferentially adsorbs on the mica surfaces. Homopolymer PS has been shown not to adsorb onto mica from toluene below solution concentrations of 1 mg/mL.[26] Because the concentration of block copolymer was held well below this value (0.06 mg/mL),

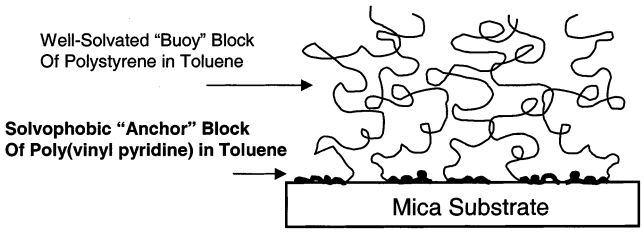

Figure 1. Depiction of the PS/PVP self-assembled layer onto mica from toluene.

the PS chains were assumed to have a purely repulsive interaction with the mica substrate and stretch away from the surface into the solvent. The architecture of the chains allowed a high enough tethering density to form the polymer brush microstructure implied by Figure 1 in most, but not all, cases.[27] Lateral heterogeneity has been found to exist for self-assembled block copolymer structures using AFM in several studies, but the SFA force-measuring device is insensitive to the scale of this heterogeneity.[27,28] The normal and lateral force measurements should, therefore, be considered averaged quantities over areas of high and low polymer tethering density.

Force Measurements. A Mark II surface forces apparatus (SFA) was used for the direct force measurements between the opposing adsorbed polymer layers. With this technique, the separation distance can be measured with a resolution of 2−3 Å. As a result of this accuracy, normal forces on the order of 0.1−1.0 μN can be detected. The device itself is placed on a vibration isolation table inside of a specially designed enclosure to precisely control the surrounding temperature and reduce thermal fluctuations. The enclosure is small in volume and made out of double-walled and insulated opaque polycarbonate. The temperature inside the enclosure could be controlled to ±0.05 °C within the range 25−45 °C using a PID controller and heating elements.

After completion of both the normal and shear force curves in toluene, the solvent quality was reduced by replacing toluene (good solvent) with cyclohexane (near-Θ solvent). This was accomplished by bringing the surfaces close together and then draining the toluene from the chamber. Capillary tension trapped a column of toluene between the surfaces, ensuring the layers were never directly exposed to any contaminates that may have been present at the solvent/air interface. The chamber was then refilled with redistilled, filtered cyclohexane (HPLC grade). The surfaces were then pumped up and down using a coarse motor to help ensure the cyclohexane was able to replace the remaining toluene in the polymer layers. The small amount of toluene remaining in the box (about 0.1 mL of toluene compared to 350 mL of cyclohexane) was assumed not to have any significant effect upon the measured force curves. After all force measurements were taken in cyclohexane, toluene was reintroduced to the SFA, and both normal and shear force curves were obtained to make sure the brush structure had not been permanently altered through the solvent exchange procedure.

Our adaptation of the SFA for investigating the dynamic response of polymer layers is based upon the design of Homola and Israelachvili[30] and has been discussed extensively in other publications.[6−8,27−29] Briefly, a piezoelectric bimorph device drives the lower surface laterally past the upper surface in an extremely parallel fashion. The careful calibration of the piezoelectric driver using scanning electron microscopy provides a means of converting the input voltage to shear amplitude. For these experiments, the lower surface was driven with a triangular ramp function to maintain a constant shear rate at a given separation distance. By adjustment of the amplitude, frequency, and separation distance between the surfaces, this shear rate may be varied. Normal force measurements were taken while the lower surface was stationary. After the normal force data was recorded, the lower surface was set in motion. The shear force was measured by monitoring how much of the lower surface motion was translated relative to the upper surface. A previously calibrated differential capacitor at the upper surface provides a sensitivity of approximately 1−10 μN in the measurement of this shear force. To ensure that the shearing motion did not change the separation distance between the two surfaces, relatively low amplitude measurements were performed (less than 500 nm in all cases). This range of amplitudes corresponds to an applied strain of order 1. The maximum deviation in the gap thickness during the applied shear did not exceed more than approximately 5 Å as measured by monitoring the position of the interference fringes. While following this criterion, it was observed that the normal forces measured while the lower surface was moving were identical to those measured while the lower surface was stationary.

This level of parallel motion was achieved through three distinct experimental steps that progressively improved the alignment during shear. First, the piezocrystal elements were sectored in such a way as to cause an "S-shaped" deflection of the lower surface, rather than the typical "C-shaped" deflection that tends to move the attached surface in an arcing motion. Second, several spots on the same sample were surveyed under shear before finding areas that would offer minimal change in separation distance with shearing motion. Spots where a 500 nm motion would lead to a 50−100 Å change in separation distance were easily obtainable. Finally, very fine adjustments in the angle of the upper surface were made by adjusting the tension of the bracket holding the upper surface against its O-ring seal. These delicate adjustments were made while the lower surface was in motion and the results were viewed in realtime by monitoring the interference pattern to see if any motion could be detected. Using this approach, changes in the separation distance could slowly be reduced down to a level of 5−25 Å over a 500 nm applied motion. Of the data obtained, only those measurements with approximately a 5 Å change are reported here. Unlike previous experiments obtained under a significant load where bending of the force measuring spring would mask any nonparallel motion, this level of alignment was achieved under zero applied load. This is very significant, because it means the normal force between the moving surfaces was constant during the measurement of the shear force. In fact, the level of parallel motion is clearly apparent when one compares the stationary normal force profiles to those obtained while the lower surface is moving. If the motion were not extremely parallel, the additional bending of the force measuring spring when the surfaces were compressed would lead to a force profile exhibiting an increased normal load under shear at a given separation distance.

The frequency range that could be explored with the SFA in our lab while monitoring the shear force was limited to between 0.01 and 1 Hz. At each separation distance, the shear force was recorded by averaging the signal over a minimum of three cycles of side-to-side motion. At 0.01 Hz, this required about 5 min for each data point. Thermal drift present in the apparatus was minimal due to the use of a specially built enclosure for the SFA, but could lead to changes in the separation distance between the opposing brushes at a rate of 2−3 Å per minute. At 0.01 Hz, therefore, the gap width could vary by as much as 15 Å during the course of a single measurement. This does not seem like much, but after a study of the data that follows, it is apparent that the shear force varies significantly with compression, and even a 15 Å change in the separation distance could alter the measurement. As a result, the frequency of 0.01 Hz was set as a lower limit to avoid this complication. Above frequencies of 1 Hz, the chart recorder used to record the shear force could not mechanically respond quickly enough to the signal sent by the amplifier. All sets of data shown represent several (at least three) trials at the same spot of the sample.

Simulation Technique. The adaptation of a single chain Brownian dynamics algorithm to a one-sided polymer brush has been extensively discussed by Doyle et al.[31] We shall only highlight here the important features and present additional details required for the simulation of two opposing brushes. The brush consists of N_{chains} chains of N beads each. The polymer model used is the bead−rod chain where successive

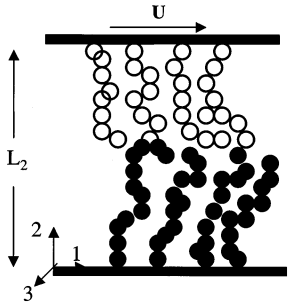

Figure 2. Image of the brush simulation geometry.

beads along a chain are held at a constant distance a from each other. The length of the rod, a, serves as the fundamental length scale in the problem, and it corresponds to the Kuhn step of the polymer. The geometry that we will be discussing exclusively is that of a polymer brush confined between two planar, smooth, impenetrable walls. Figure 2 shows the schematic of a two-brush system. This geometry is similar to that of experiments using SFA, where the polymers are trapped between two mica-covered crossed cylinders whose radii-of-curvature are much greater than the gap width.

For the remainder of this paper, all simulation parameters and results will be given in dimensionless terms unless otherwise stated. Length is measured in units of the Kuhn step, a; time is measured in units of the bead diffusion time, $\zeta a^2/kT$, where ζ is the drag on a bead, kT is the thermal energy, and force is measured in units of kT/a. The simulation domain considered is a rectangular box of dimensions L_1, L_2, L_3. For a steady shear flow, we adopt the convention that the "1" axis is the direction of the flow, "2" the direction of the velocity gradient, and "3" the direction of vorticity (cf. Figure 2). Before commencing a simulation, we need to specify other parameters, and they are N, the number of beads per chain, N_{chains}, the number of chains, and σ, the grafting density defined as the number of chains per area, i.e., $N_{\text{chains}}/(L_1L_3)$. Periodic boundary conditions have been used in the "1" and "3" directions in order to simulate an infinite, planar brush. Finally, the time step sizes used for all the simulations vary from $\Delta t = 5 \times 10^{-4}$ to 5×10^{-3} measured in units of the bead diffusion time, $\zeta a^2/kT$.

Calculating the Solvent Velocity in the Brush. In our simulations, a shear flow is achieved by introducing a boundary condition that is equivalent to moving the top plate at a constant velocity. Because the force exerted by the tethered polymers on the solvent is determined by the polymer configuration which, in turn, is dependent on the surrounding solvent flow, the solvent velocity profile is calculated self-consistently[31] between the force density calculated from Brownian dynamics simulations and the equation of momentum conservation for Stokes flow (Brinkman type equation) given by the following equation:

$$\frac{1}{3\pi}\frac{\partial^2\langle u_i\rangle}{\partial x_i \partial x_i} - \frac{\partial\langle P\rangle}{\partial x_i} + \langle f_i(x_i,t;u_i)\rangle = 0 \qquad (1)$$

$\langle u_i\rangle$ is the averaged solvent velocity (made dimensionless with $kT/\zeta a$), $\langle P\rangle$ is the averaged dynamic pressure, $\langle f_i\rangle$ is the averaged force density exerted by the brush on the solvent, and x_i is the position vector.

Incorporating Solvent Quality and Determining the Θ Point of the Chain. The interaction potential that we have used is the truncated Lennard-Jones interaction given in dimensionless form as the following equation:

$$E(r) = \begin{cases} 4\epsilon[r^{-12} - r^{-6} - r_c^{-12} + r_c^{-6}] & r \le r_c \\ 0 & r > r_c \end{cases} \qquad (2)$$

where the potential energy, E, and the depth of the well, ϵ, have been made dimensionless by the thermal energy kT, and the distance between bead centers, r, and the interaction cutoff radius, r_c, have been made dimensionless with the collision diameter, d (which is set equal to the bead size, a).[32] The cutoff radius has been set at $2.5a$. To establish a Θ point so that we can distinguish between a good and a poor solvent, we calculate the interbead second virial coefficient, v, defined (in dimensionless terms) by the following equation:

$$v = 2\pi\int_0^\infty [1 - \exp(-E(r))]\, r^2 dr \qquad (3)$$

Here we use the LJ potential for $E(r)$ and vary the depth of the potential well, ϵ, until $v = 0$.[33] Using this method, we find that at $\epsilon = 0.293$ v vanishes, and we shall call this energy the Θ point for our bead−rod chain. For ϵ greater than 0.293, v is negative, and we have a poor solvent. Conversely, for ϵ less than 0.293, v is positive, and we have a good solvent. However, a more computationally efficient way to simulate a good solvent is to include only the repulsive part of the potential,[34] i.e., set r_c at $2^{1/6}$, and this method corresponds to simulating the athermal solvent limit. We note that according to Graessley et al.[35] even the "best" experimental good solvents do not correspond to the athermal limit. We note that Graessley et al. simulated the Θ point of a freely jointed (untethered) chain using off-lattice Monte Carlo methods and found the Θ temperature to be 0.318. This value is very close to the one we found using the method described above. This Θ point is only strictly valid, however, for a free chain in dilute solution. As a result, this choice of ϵ will correspond to near-Θ conditions inside a polymer brush. However, in the present study we are interested in a qualitative comparison between the good and Θ solvent regimes. Thus, our comparison between experiments and simulations are valid so long as we are comparing between brushes in a good and near-Θ regimes in both cases.

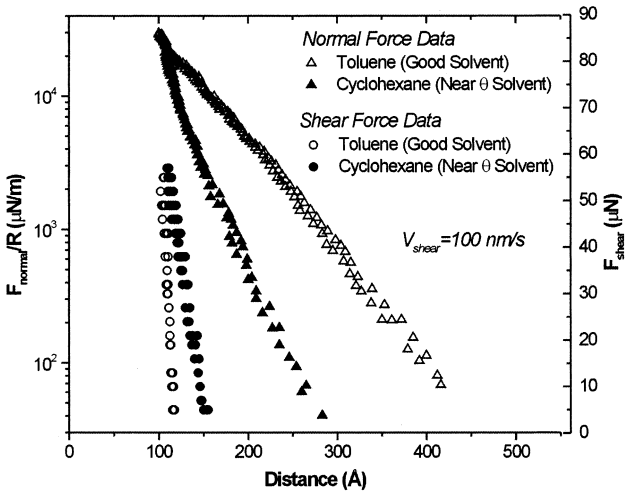

Figure 3. Plot of the normal and shear forces between PS/PVP [25/4]k brushes as a function of compression and solvent quality. The shearing velocity was held constant at 100 nm/s.

Results and Discussion

Adsorbed Layer Structure and Normal Forces. Experimental data was acquired on two different PS/PVP systems and the force profiles obtained are shown in Figures 3 and 4. For clarity, the normal force data is illustrated on a log scale and the shear force data on a linear scale. Also notice that the Derjaguin approximation[36] has been applied to normalize the normal force data, while the shear force data has been reported without normalization. The number of PS repeat units, N_{PS}, the equivalent radius of gyration of an untethered PS chain, $R_{g,\text{PS}}$, the surface area per tethered chain, A, the overlap density, $\sigma^* = \pi R_{g,\text{PS}}^2/A$, and the solvated PS layer thickness, L_o, for the different PS/PVP molecules in both toluene and cyclohexane are reported in Table 2. The layer thickness was obtained by setting

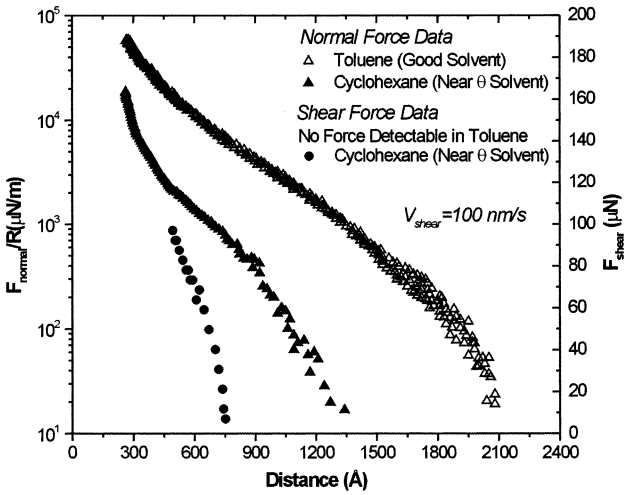

Figure 4. Plot of the normal and shear forces between PS/PVP [255/24]k brushes as a function of compression and solvent quality. The shearing velocity was held constant at 100 nm/s.

Table 2. Tethered Layer Characterization

name	A (Å^2)	N_{PS}	$R_{g,PS}$ (Å)	L_o (Å)	σ^*	$L_o/R_{g,PS}$
Toluene at 32 °C (Good Solvent)						
PS/PVP[25/4]k	2630	239	52[a]	220	3.3	4.2
PS/PVP[255/24]k	13 900	2453	199[a]	1015	8.9	5.1
Cyclohexane at 32 °C (Near-Θ Solvent)						
PS/PVP[25/4]k	2630	239	46[a]	145	2.5	3.2
PS/PVP[255/24]k	13 900	2453	151[a]	650	5.2	4.3

[a] On the basis of experimental data from ref 22.

the separation distance at the onset of normal forces, D^*, equal to $2L_o$. The value of A was determined from the dry PS/PVP layer thickness, L_{dry}, using the technique of Kilbey et al.[37] As expected, the normal forces between the tethered PS chains shift to smaller separation distances and become steeper as the solvent quality is worsened. The reason for this is that the osmotic driving force for stretching of the chains is reduced, which leads to a shorter, more compact layer structure. Although not shown here, the normal force curves between these and other end-tethered PS/PVP systems can be collapsed onto a single universal curve in both good and near-Θ solvents following the brush scaling theory of Patel et al.[38] In addition, the normal force data in a good solvent can be predicted a priori using the SCF brush approach of Milner.[39] Both of these findings, coupled with the fact that $L_o > R_{g,PS}$ in all cases, verify the brush picture inferred by Figure 1 and allow us to use brush scaling arguments to model the shear forces between the PS/PVP layers. Another important observation is that the compression and expansion cycles were completely reproducible in both toluene and cyclohexane. The lack of a crushing hysteresis, as might be observed on homopolymer PS layers, argues against PS adsorption onto mica in the presence of cyclohexane. The reversible nature of the experiment upon changing solvents suggests that no permanent structural changes occurred using our solvent exchange procedure.

After static normal force curves were obtained, the lower surface was set in motion and the normal and shear forces between the layers were measured. The velocity used during the course of these experiments was held constant and was calculated directly from the applied peak-to-peak amplitude and frequency. The same velocity was used in both the good and Θ solvent cases for both PS/PVP systems. Since the separation distance changes with compression, the shear rate will vary over the course of the experiment as the layers are squeezed. This variation will be nonlinear with changes in the gap width, since the permeability of the tethered layers will change with compression.[10] Because of these inherent vagaries, the shear rate was not estimated and no attempt was made to maintain a constant shear rate during the experiments. No differences were observed between the static normal force data and the normal force data obtained while the lower surface was in motion. As mentioned before, this is an indication of the extremely parallel nature of the shearing motion, since any changes in separation distance induced by misalignment will lead to additional normal forces being measured in the SFA experiment. This observation also suggests that the shearing motion did not lead to the ejection of chains from the gap or any other type of permanent damage to the end-tethered layers.

The toluene data in Figures 3 and 4 demonstrate that the polystyrene brushes are capable of supporting extremely large loads in a good solvent before a shear force greater than 1 μN is transmitted between them. From a practical point of view, the swollen polymer layers in a good solvent act as highly efficient lubricating agents. The situation changes when the solvent quality is reduced. The normal load that needs to be applied to observe a shear force is nearly 1 order of magnitude less in a near-Θ solvent than in a good solvent. As the molecular weight of the tethered chains increases, the changes in the shear force with solvent quality become larger and more apparent. This behavior is similar to the results obtained by Kilbey,[6] and in qualitatively good agreement with the good solvent results of Klein et al.[9−11,13] and the near-Θ solvent results of Granick et al.[14−16]

This is the first study, however, to measure both the shear force in a good solvent *and* in a near-Θ solvent *on the same layers*. This dramatically reduces the number of variables that could confound comparisons, such as differences in tethering density, method of tethering, molecular weight, polydispersity, sliding amplitude, sliding frequency, etc. Because the tethering density remains constant as the solvent quality is reduced, the distance axis corresponds directly to an average polymer volume fraction in the gap following the equation: $\Phi_{PS,av} = L_{dry}/D$ where L_{dry} is the dry bilayer thickness measured at the end of the experiment. Casting the data in Figures 3 and 4 in this way allows us to say that the concentration of polystyrene necessary to obtain a detectable shear force is much lower in cyclohexane (near-Θ solvent) than in toluene (good solvent). As we will discuss later, the shear force is directly related to the effective viscosity of the material in the gap. This suggests, then, that the effective viscosity of a PS brush in toluene is much lower than the effective viscosity of a PS brush in cyclohexane at a given concentration in the semidilute regime. As previously pointed out,[6] this trend has also been observed in bulk rheology measurements of untethered PS chains in good and Θ solvents[17−20] and was related to changes in the monomeric friction factor of PS with solvent quality.[17] We believe this same mechanism plays a large role in understanding the differences in the shear forces observed with the SFA as the solvent quality is made worse. The notion that differences exist in the amount of interpenetration between the layers

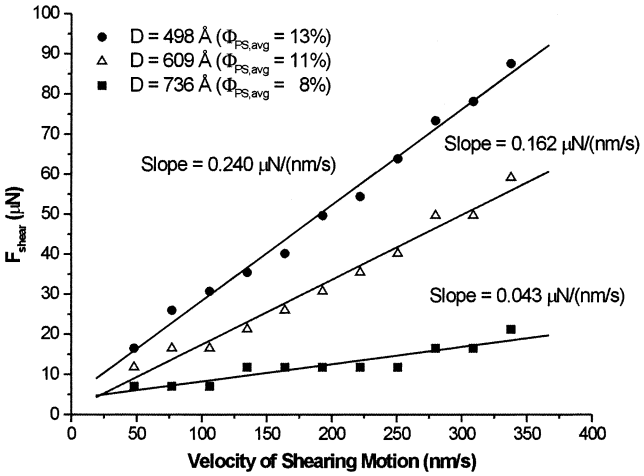

Figure 5. Plot of the effect of sliding velocity and compression on shear force between PS/PVP [255/24]k layers in cyclohexane at 32 °C.

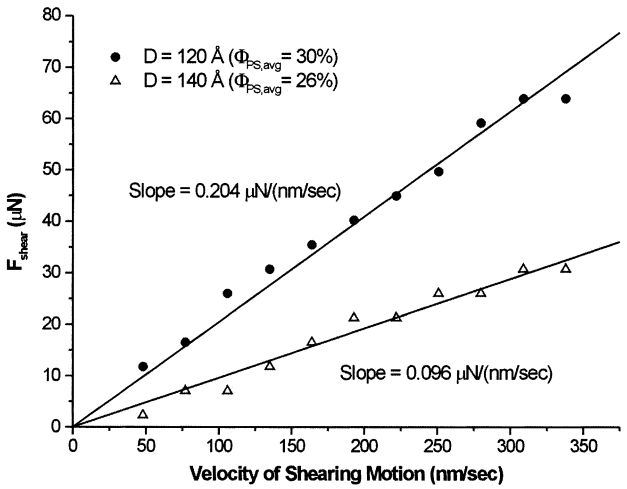

Figure 6. Plot of the effect of sliding velocity and compression on shear force between PS/PVP [25/4]k layers in cyclohexane at 32 °C.

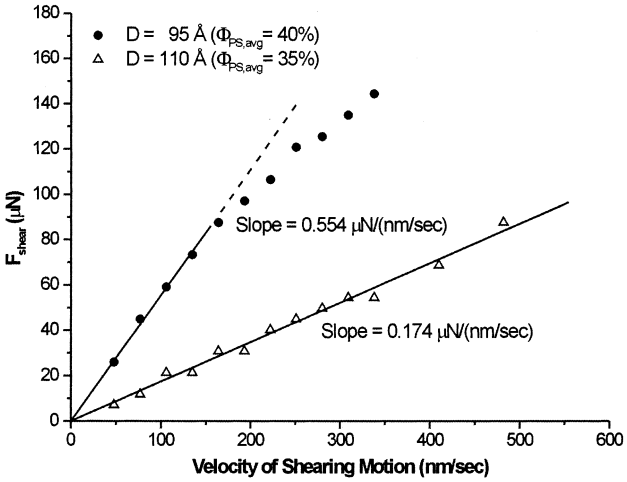

Figure 7. Plot of the effect of sliding velocity and compression on shear force between PS/PVP [25/4]k layers in toluene at 32 °C.

with solvent quality cannot be directly confirmed or denied with the SFA but will be addressed through the simulation results later in this section.

Effect of Sliding Velocity on Shear Force. In this section, we will explore the relationship between the shear force transmitted from the moving to the stationary surface via a polymer brush as a function of the imposed velocity. We will first present the experimental findings from the SFA and then the simulation results from Brownian dynamics. We note that, as far as we know, no other research group has ever presented the transition from linear to nonlinear dependence of the shear force on velocity that we have observed here. The only evidence of nonlinear behavior was reported by Grest[4,5,21] in his molecular dynamics simulation work, where he probed a very large velocity range and found nonlinear behavior at all reported gap widths. This nonlinear behavior was evidently the result of the very large imposed velocities. However, as we shall see, both our experimental and simulations results show such a shear thinning transition can be induced by confinement in addition to increasing the applied velocity.

The experimental results presented in this section are obtained from the same brushes described in the preceding section while held at different levels of compression. The simulations were developed to qualitatively model the lower molecular weight system of PS/PVP[25/4]k. The polystyrene block in this molecule is made of approximately 34 Kuhn steps,[40] while our simulations used $N = 25$ or 12.5 Kuhn steps in order to reduce the computation time. Figures 5−7 show how varying the sliding velocity and compression impacts the shear force between polystyrene brushes in good and Θ solvents. The velocity was varied by changing both the oscillating frequency between 0.01 and 1 Hz and the amplitude from 0 to 5000 Å. The reasons for these limitations on frequency and amplitude were discussed in the Experimental Section. One further limitation was that we did not attempt to measure shear forces higher than about 150 μN. This final restriction was self-imposed to prevent destruction of the polymer layer during the experiment.[13] Keeping the polymer layer intact during the shear measurements was imperative so that the dry layer thickness and tethering density could be properly measured at the end of the experiment. Over this relatively small frequency and amplitude range, the shear force measured was a function only of the sliding velocity and not of the specific combination of frequency and amplitude. This observation suggests that the relaxation time of the material in the gap was much less than 1 s.

All of the data in cyclohexane (Figures 5 and 6) and the data for low sliding velocity and low compression in toluene (Figure 7) show a linear dependence of the shear force with sliding velocity. For the extremely high compression experiments shown in Figure 7, the shear force starts to show some nonlinear behavior at higher sliding velocities. We will have more to say about this apparent shear-thinning behavior later, for now we will focus on the Newtonian limit. The slope of this linear dependence is related to the effective viscosity of the material in the gap, $\partial F/\partial V \sim \eta_{o,eff}$. To actually calculate the effective viscosity, however, requires a model for both the solvent flow width, H, and the chain length density in the solvent flow region.

Klein[11] has developed such a model for shearing polymer brushes in a good solvent that can be generalized for use in Θ solvent conditions. In his approach, a step profile model is used for the segment distribution and the measured shear force results from energy dissipation as chains are dragged through an interfacial width, δ. In other words, Klein has set the solvent flow

gap width, H, equal to the interfacial width, δ. For brushes just coming into overlap, or when the separation distance, D, is equal to twice the brush height, $2L_o$, the interfacial width, δ, was set equal to the distance between tethering points, ξ_o. For compressed brushes, Witten et al.[41] demonstrated that $\delta \approx \xi_o q^{-1/3}$ where $q = (D/2L_o)$ is the degree of compression of the brushes. Simulation results suggest that this scaling relationship works well for both good and Θ solvents.[23,24,42−44] For compressed brushes, the Alexander−de Gennes picture of close packed blobs holds well, except that the blob size ξ will depend on the average polymer concentration, ϕ_{av}. Scaling theory[45] suggests that for small changes in the concentration of a semidilute solution

$$\xi \approx \xi_o \left(\frac{\phi_{av}}{\phi_o}\right)^{\nu/(1-3\nu)} \tag{4}$$

where $\nu = {}^3/_5$ for a good solvent and ${}^1/_2$ for a Θ solvent and ϕ_o is the average polymer concentration when $D = 2L_o$. To estimate the number of blobs per chain, n, within the interfacial region, Klein points out that the mean volume occupied by each chain, V_{PS}, within δ is approximately $V_{PS} = \pi(\xi_o/2)^2(\delta/2)$ so that

$$n = \frac{\pi(\xi_o/2)^2(\delta/2)}{\xi^3} = \pi/8q^{-1/3}(\xi_o/\xi)^3 = \pi/8q^{(12\nu-1)/(3-9\nu)} \tag{5}$$

where eq 4 and the identity[11] $q = \phi_o/\phi_{av}$ have been used to obtain the final expression. When the brushes are sheared, each chain is dragged through the effective medium of the other chains in the interfacial region. For blobs behaving hydrodynamically as nonfree-draining spheres (so-called Zimm blobs), the resulting shear stress, σ_s, is given by Klein as

$$\sigma_s = (\text{chains/area}) \times (\text{blobs per chain in interfacial zone}) \times (\text{drag per blob}) = (1/\xi_o^2)(n)(6\pi\eta_{eff}U\xi) \tag{6}$$

where the last term is the Stokes drag on a blob of size ξ moving at velocity U in a medium of effective viscosity η_{eff}. The assumption of nonfree-draining blobs should be valid in both good and Θ solvents as long as $\delta/U > \tau_{z,b}$, where $\tau_{z,b}$ is the relaxation rate of a Zimm blob on the order of 10^{-6} s.[11] Substituting for ξ and n in eq 6 and multiplying the shear stress by the interaction area, A_{eff}, leads to the following expression for the shear force:

$$F_{shear} = \sigma_s A_{eff} = \left(\frac{12\pi^2 R_c L_o}{\xi_o}\right) q^{2/(3-9\nu)} \eta_{eff} U \tag{7}$$

Here the interaction area between the crossed cylindrical surfaces in the SFA possessing an average radius-of-curvature R_c was estimated using the Langbein approximation.[46] The effective zero-shear viscosity of the material in the gap can then be calculated from the slope of the shear force dependence on velocity in the linear viscoelastic regime:

$$\eta_{o,eff} = \eta_{eff}|_{U\to 0} = \left[\left(\frac{12\pi^2 R_c L_o}{\xi_o}\right) q^{2/(3-9\nu)}\right]^{-1} (\partial F_{shear}/\partial U) \tag{8}$$

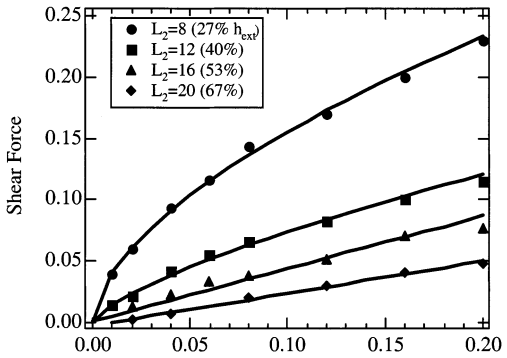

Figure 8. Plot of shear force vs velocity in good (Figure 8) solvents at various compressions (h_{ext} is the simulated equilibrium brush height). In a good solvent, the shear force grows linearly with velocity for compressions at or below 53%.

Table 3. Model Calculation Results for PS/PVP Interfacial Viscosity at 32 °C

sample	solvent	D (Å)	$q = D/2L_o$	ϕ_{av} (% PS)	$\eta_{o,eff}$ (Pa s)
PS/PVP[255/24]k	cyclohexane	736	0.57	8	3.8
PS/PVP[255/24]k	cyclohexane	609	0.47	11	11
PS/PVP[255/24]k	cyclohexane	498	0.38	13	13
PS/PVP[25/4]k	cyclohexane	140	0.48	26	5.3
PS/PVP[25/4]k	cyclohexane	120	0.41	30	9.1
PS/PVP[25/4]k	toluene	110	0.25	35	6.2
PS/PVP[25/4]k	toluene	95	0.22	40	18

Equation 8 has been applied to the experimental results obtained in Figures 5−7. The resulting effective zero-shear viscosities, along with the average polymer concentration in the gap, are reported in Table 3.

Some of the trends observed for the data in Table 3 directly parallel what one might expect for a bulk rheology experiment on a semidilute polymer solution. First, the calculated zero-shear viscosity increases with polymer concentration (compression) for a given molecular weight. Second, the effective viscosity also increases with molecular weight at a given polymer concentration. The increase in solution viscosity with decreasing solvent quality at a given polymer concentration and molecular weight has also been observed previously in the literature.[17−20] Again, we believe the same mechanism that leads to increased viscosity in bulk rheology experiments on PS gives rise to the increased shear force measured with the SFA in these and other experiments. Quantitatively comparing the effective viscosities reported in Table 3 with bulk rheology data on PS in toluene and cyclohexane at the same molecular weight and polymer concentration,[17] we find that the values calculated here are 1−2 orders of magnitude larger than those for free chains. This is in agreement with recent simulation results comparing the rheological properties of end-tethered to free chains.[47]

Having shown the SFA results for the shear force vs velocity, we now turn to the simulation predictions under analogous conditions. Figures 8 and 9 show the shear force as a function of velocity over a range of compressions for good and Θ solvents, respectively. Comparing the experimental (Figures 5−7) and simulation (Figures 8 and 9) results, we see very good qualitative agreement. Both sets of data reveal a linear dependence of the shear force on velocity for large gap widths (or small compressions). However, as the gap width decreases, a nonlinear behavior emerges. Because of the self-imposed limit on the measured shear force in the SFA, we could not compress the brushes in

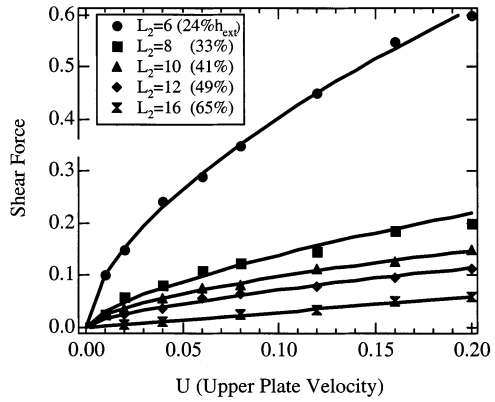

Figure 9. Plot of shear force vs velocity in near-Θ solvents at various compressions (h_{ext} is the simulated equilibrium brush height). In a near-Θ solvent, the trend is linear at 65% compression.

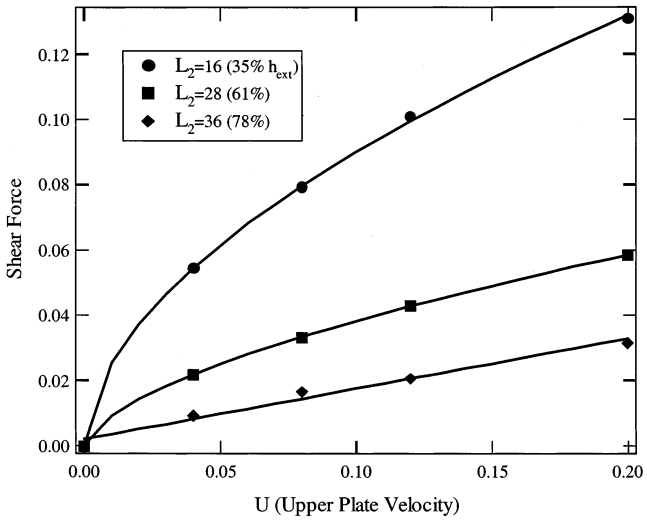

Figure 10. Plot of shear force vs velocity in a good solvent for $N = 40$ (at the same surface density as for $N = 25$).

cyclohexane further than shown in Figures 5 and 6. As a result, we were unable to observe a transition from linear to sublinear behavior in a near-Θ solvent. However, that transition is observed in the case of the good solvent (Figure 7) and is consistent with the simulation results. Thus, both experiments and simulations indicate that nonlinear viscoelastic behavior in a polymer brush can be achieved not only by increasing the imposed velocity but also by increasing confinement. (In Figure 10, we show the results of the shear force vs velocity results for brushes formed from much longer chains, $N = 40$ beads (or about 20 Kuhn steps) in a good solvent. Again, we observe a transition from a linear regime (78% compression) to a nonlinear one (starting at 61% on the figure). Thus, we believe that this linear to nonlinear transition is independent of chain size but inherent to the response of a brush under shear.)

One possible explanation for the transition from linear to sublinear dependence of the shear force on the velocity is a decrease in the width of the interpenetration zone. Figures 11 and 12 show the interfacial width, δ, normalized by the equilibrium value at the respective gap width in good and Θ solvents. In both cases, we see that δ decreases monotonically with increasing velocity. In the case of the good solvent, we observe that δ decreases most rapidly at the highest compression ($L_2 = 8$) over the range of velocities sampled and that

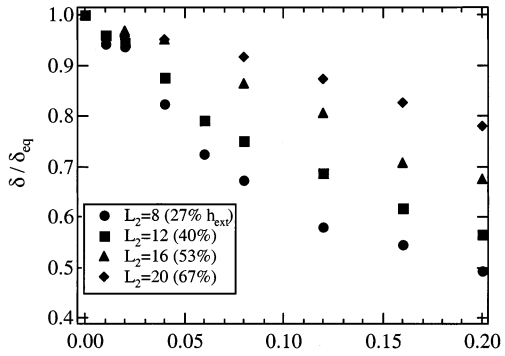

Figure 11. Plot of the interfacial width normalized by the equilibrium value vs velocity at various compressions for a good solvent.

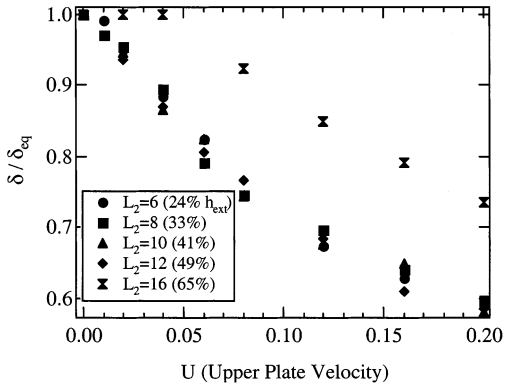

Figure 12. Plot of the interfacial width normalized by the equilibrium value vs velocity at various compressions for a near-Θ solvent.

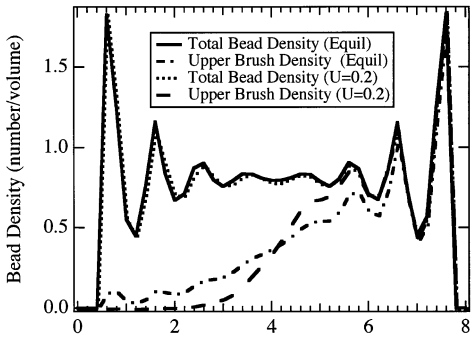

Figure 13. Plot of the bead density profile at equilibrium and at $U = 0.2$ in a good solvent, for 27% compression ($L_2 = 8$).

the rate at which δ decreases lessens as the degree of compression is reduced. For the case of the Θ solvent, except for the smallest compression ($L_2 = 16$), all the values of δ seem to collapse onto the same curve. On a physical basis, the reason for the decrease in the width of the interpenetration zone as the velocity increases is that the chains of the opposing brushes tend to align and tilt in the flow direction. This causes the tail of the opposing brushes to retract toward their respective tethering plane and, consequently, to reduce the region of overlap between the two brushes. Figures 13 and 14 show the bead density profile of two opposing brushes in a good solvent at equilibrium and at a velocity of $U = 0.2$ at two different compressions. Both the overall as well as the upper brush density profiles are shown. Comparing the upper brush density profile at equilibrium and $U = 0.2$, we clearly see that when sheared, the tail of the brush retracts. Furthermore, this tail retraction is more pronounced at higher compressions.

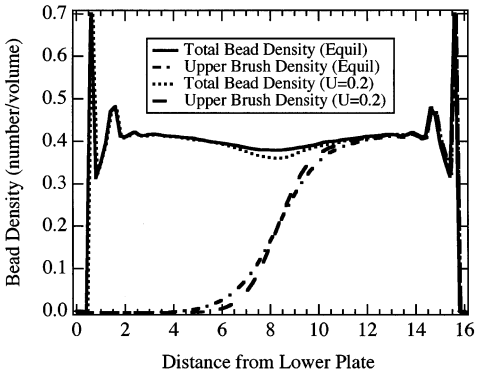

Figure 14. Plot of the bead density profile at equilibrium and at $U = 0.2$ in a good solvent for 53% compression ($L_2 = 16$).

In other words, a significant decrease in δ (due to increasing compression or velocity) will cause the number of beads in the interfacial region to decrease. Since shear forces arise from the collisions of the beads of the opposing brushes in the interfacial region, this reduction in interfacial beads with velocity will lead to a sublinear dependence of the shear force with the imposed velocity. We note that this chain retraction under strong shear was also observed by Grest in his study of brushes using molecular dynamics.[5]

Conclusions

The shear forces between neutral polymer chains tethered to opposing interfaces have been measured with the SFA in both good and Θ solvents. When the shearing velocity was varied, the complex polymer/solvent system found at the interface between the opposing layers responded at low and medium speeds and compressions with the shear force increasing linearly with the shear velocity. The effective viscosity of the material in the interfacial region was estimated using a scaling approach suggested by Klein et al and found to be 1−2 orders of magnitude larger than the viscosity of free chains in semidilute solutions. This result is in agreement with the computer simulations of Lemak et al.[47] that demonstrate a viscosity enhancement of chains tethered to an interface. At larger shear velocities or higher extents of compression, Brownian dynamics simulations suggest the interfacial width will thin, leading to a sublinear increase in the shear force with sliding velocity. Experimental limitations prevented us from looking at extremely large shear velocities, but confinement eventually did lead to sublinear behavior, in agreement with the simulation prediction.

Acknowledgment. We acknowledge support for this work from several sources within the NSF: the Interfacial Transport and Separations Program (NSF-CTS-9816147 and NSF-CTS-9616797), CPIMA Cooperative Agreement No. DMR-9400354-2, and the Graduate Research Fellowship program. P.A.S. would also like to thank Dr. Ken Hanley and Professor Timothy Lodge at the University of Minnesota for their help in the syntheses of the block copolymers used in this study.

References and Notes

(1) Klein, J.; Kumacheva, E. *J. Chem. Phys.* **1998**, *108*, 6996−7009.
(2) Klein, J. *J. Non-Cryst. Solids* **1998**, *235−237*, 422−427.
(3) Kumacheva, E.; Klein, J. *J. Chem. Phys.* **1998**, *108*, 7010−7022.
(4) Grest, G. S. *Curr. Opin. Colloidal Interface Sci.* **1997**, *2*, 271−277.
(5) Grest, G. S. *Adv. Polym. Sci.* **1998**, *138*, 149−183.
(6) Kilbey, S. M., II. Dynamic Behavior of Block Copolymers. Ph.D. Thesis, University of Minnesota, Minneapolis, MN, 1996.
(7) Kilbey, S. M., II; Schorr, P. A.; Tirrell, M. Frictional Behavior of Self-Assembled Polymer Brushes. In *Molecular Interactions and Time-Space Organization in Macromolecular Systems*; Morishima, Y., Norisuye, T., Tashiro, K., Eds.; Springer: New York, 1998.
(8) Kilbey, S. M., II; Schorr, P. A.; Tirrell, M. Effect of Solvent Condition on the Dynamic Response of Polymer Brushes In *Dynamics of Small Confining Systems IV*; Drake, J. M., Grest, G. S., Klafter, J., Kopelman, R., Eds.; Materials Research Society: Pittsburgh, PA, 1999.
(9) Klein, J.; Kumacheva, E.; Mahalu, D.; Perahia, D.; Fetters, L. J. *Nature (London)* **1994**, *370*, 634.
(10) Klein, J.; Kamiyama, Y.; Yoshizawa, H.; Israelachvili, J. N.; Fredrickson, G. H.; Pincus, P.; Fetters, L. J. *Macromolecules* **1993**, *26*, 5552−5560.
(11) Klein, J. *Annu. Rev. Mater. Sci.* **1996**, *26*, 581−612.
(12) Pelletier, E.; Belder, G. F.; Hadziioannou, G.; Subbotin, A. *J. Phys. II (Fr.)* **1997**, *7*, 271−283.
(13) Klein, J.; Kumacheva, E.; Perahia, D.; Fetters, L. J. *Acta Polym.* **1998**, *49*, 617−625.
(14) Cai, L. L.; Peanasky, J.; Granick, S. *Trends Polym. Sci.* **1996**, *4*, 47−53.
(15) Dhinojwala, A.; Cai, L.; Granick, S. *Langmuir* **1996**, *12*, 4537−4542.
(16) Granick, S.; Demirel, A. L.; Cai, L. L.; Penansky, J. *Isr. J. Chem.* **1995**, *35*, 75−84.
(17) Ghandi, K. S.; Williams, M. C. *J. Polym. Sci.: Part C* **1971**, *35*, 211−234.
(18) Tager, A. A.; Dreval, V. E.; Lutsky, M. S.; Vinogradov, G. V. *J. Polym. Sci.: Part C* **1968**, *23*, 181−194.
(19) Ultracki, L.; Simha, R. *J. Polym. Sci.* **1963**, *1*, 1089−1100.
(20) Simha, R.; Utracki, L. *J. Polym. Sci.: Part A2* **1967**, *5*, 853−866.
(21) Grest, G. S. *Mater. Res. Soc. Symp. Proc.* **1997**, *464*, 71−82.
(22) Kreer, T.; Muser M. H.; Binder, K.; Klein, J. *Langmuir* **2001**, *17*, 7804−7813.
(23) Levicky, R. Polymer Brushes and Mesogels in Selectively Swollen Block Copolymer Films. Ph.D. Thesis, University of Minnesota, Minneapolis, MN, 1996.
(24) Pelletier, E.; Stamouli, A.; Belder, G.; Hadziioannou, G. *Langmuir* **1997**, *13*, 1884−1886.
(25) Antonietti, M.; Heinz, S.; Schmidt, M.; Rosenauer, C. *Macromolecules* **1994**, *27*, 3276−3281.
(26) Thambo, G.; Miller, W. *Macromolecules* **1990**, *23*, 4397−4403.
(27) Schorr, P. A. Equilibrium and Dynamic Properties of Tethered Polymer Chains. Ph.D. Thesis, University of Minnesota, Minneapolis, MN, 2000.
(28) Kelley, T. W.; Schorr, P. A.; Johnson, J. D.; Tirrell, M.; Frisbie, C. D. *Macromolecules* **1998**, *31*, 4297−4300.
(29) Kilbey, S. M.; Bates, F. S.; Tirrell, M.; Yoshizawa, H.; Hill, R.; Israelachvili, J. *Macromolecules* **1995**, *28*, 5626−5631.
(30) Homola, A. M.; Israelachvili, J. N.; Gee, M. L.; McGuiggan, P. M. *J. Tribol.* **1989**, *111*, 675.
(31) Doyle, P. S.; Shaqfeh, E. S. G.; Gast, A. P. *Macromolecules* **1998**, *31*, 5474−5486.
(32) Rowley, R. L. *Statistical Mechanics for Thermophysical Property Calculations*; Prentice Hall: Upper Saddle River, NJ, 1994.
(33) McQuarrie, D. A. *Statistical Thermodynamics.* University Science Books, Mill Valley, CA 1973.
(34) Grest, G. S.; Murat, M. *Macromolecules* **1993**, *26*, 3108−3117.
(35) Graessley, W. W.; Hayward, R. C.; Grest, G. S. *Macromolecules* **1999**, *32*, 3510−3517.
(36) Derjaguin, B. V. *Z. Kolloid* **1934**, *69*, 155−164.
(37) Kilbey, S. M., II; Watanabe, H.; Tirrell, M. *Macromolecules* **2001**, *34*, 5249−5259.
(38) Patel, S.; Tirrell, M. *Colloids Surf.* **1988**, *31*, 157−179.
(39) Milner, S. T. *Europhys. Lett.* **1988**, *7*, 695−699.
(40) Li, L.; Larson, R. G.; Sridhar, T. *J. Rheol.* **2000**, *44*, 291−322.
(41) Witten, T. A.; Leibler, L.; Pincus, P. A. *Macromolecules* **1990**, *23*, 824−829.
(42) Hirz, S. J. Modeling Interactions between Adsorbed Block Copolymers. Ph.D. Thesis, University of Minnesota, Minneapolis, MN, 1986.
(43) Shim, D. F. K.; Cates, M. E. *J. Phys.* **1990**, *51*, 701−707.
(44) Murat, M.; Grest, G. S. *Phys. Rev. Lett.* **1989**, *63*, 1074−1077.

(45) de Gennes, P. G. *Scaling Concepts in Polymer Physics*; Cornell University Press: New York, 1979.
(46) Israelachvili, J. N. *Intermolecular and Surface Forces*; Academic Press: San Diego, CA, 1992.
(47) Lemak, A.; Balabaev, N.; Karnet, Y.; Yanovsky, Y. *J. Chem. Phys.* **1998**, *108*, 797−806.

MA011207V